HIGH $k_t^2 \times Q$, MULTI-FREQUENCY LITHIUM NIOBATE RESONATORS

Renyuan Wang[1], Sunil A. Bhave[1], and Kushal Bhattacharjee[2]
[1]Cornell University, USA
[2]RF Micro Devices, Inc., USA

ABSTRACT

This paper presents design and vacuum measurements of lithium niobate (LN) contour-mode resonators (CMR). By carefully positioning the inter-digital transducer (IDT), we achieved CMRs with $k_t^2 \times Q$ of 7%*2150=148 (IDT @ node) or resonators with very high k_t^2 of 12.3% and spur-attenuated response (IDT @ anti-node). In addition, we demonstrated resonators with frequencies ranging from 400MHz to 800MHz on a single chip.

INTRODUCTION

Motivation

To satisfy the ever-increasing demand for spectrum, commercial markets desire integrated multi-frequency "band"-select duplexer and diplexer filters, with fractional bandwidth (BW) ranging from 3% to 10% and steep roll-off for high stop band rejection. In the past decade, MEMS filters and surface-acoustic-wave filters have dominated the duplexer and diplexer markets. Such filters consist of a ladder network of multiple MEMS resonators or surface-acoustic-wave (SAW) resonators. The achievable bandwidth of such filter is ultimately limited by the electro-mechanical coupling factor (k_t^2) of the resonators, while the roll-off is determined by resonator quality factor (Q). Therefore, resonators with both high k_t^2 and high Q are desired for large BW, steep roll off band-pass filters.

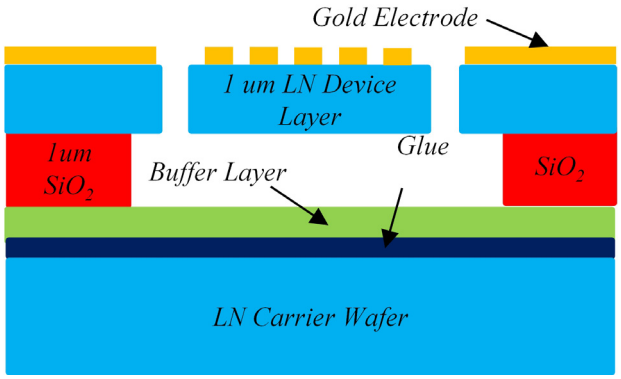

Figure 1: Schematic cross-section of the resonator.

Traditional electrostatic drive MEMS resonators have shown very high quality factor [1], but suffer from extremely low k_t^2, due to the poor transduction efficiency of the electrostatic actuator. Filters based on Aluminum Nitride (AlN) film bulk-acoustic-wave resonators (FBARs) have demonstrated 7% BW [2], however it is not suitable for multi-frequency integration as the resonant frequency is defined by the thickness of the AlN thin-film. On the other hand, their multi-frequency contour-mode counterparts are limited to <2.5% BW [3] due to the small d_{31} piezoelectric strain coefficient of sputtered AlN. Consequently, while FBAR filters have dominated the CDMA market, filters based on contour-mode AlN resonators have struggled to find a firm footing. Lithium Niobate (LN) based multi-frequency SAW filters have shown very large k_t^2 and BW [4]. But due to the one dimensional acoustic energy confinement in SAW configuration, energy is easily dissipated in the transverse direction as well as vertically through the substrate, which leads to low Q and parasitic modes.

To leverage the high coupling coefficient of LN with the high quality factor from mode-isolation and energy trapping of released and undercut mechanical structures, LN contour mode resonators have been proposed [5,6]. However, the initial results only showed moderate Q and k_t^2 with IDT placed at mechanical nodes, which is similar to AlN CMR. In this paper, we present resonators with high Q or large k_t^2 with spur-attenuated response by carefully positioning the inter-digital transducer (IDT) at different locations. In addition, we discuss the necessity of performing vacuum measurement to achieve high quality factor from LN CMRs.

DEVICE CONCEPT

Fabrication

Fig. 1 shows the final cross section of the resonators, where the device is excited to vibrate laterally in high-

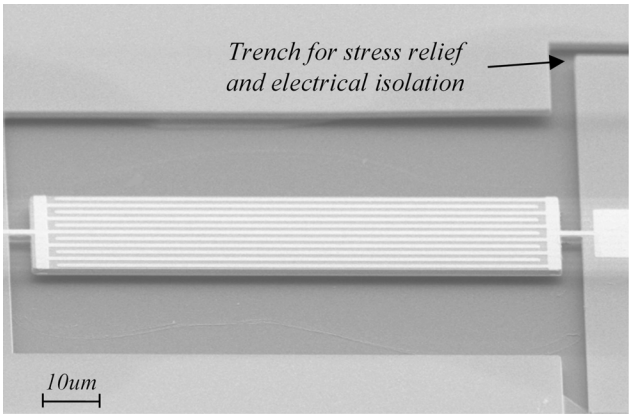

Figure 2: SEM of a 90um x 40um LN contour-mode resonator with 11 finger electrodes.

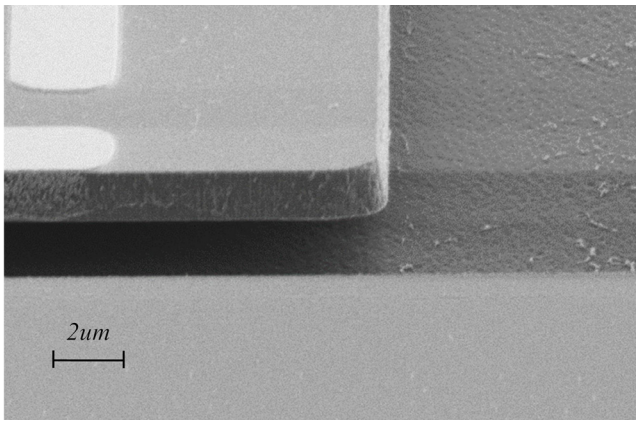

Figure 3: Zoom-in SEM of the ion-milled side-wall profile of the final resonator.

order contour mode by top gold IDT. The devices (Fig.2) are fabricated on a stack of LN thin-film (Y136-cut), SiO_2 release layer and a buffer layer bonded to a LN handle wafer using glue [5]. The device geometry is defined using ion-mill. As shown in Fig. 3, the ion-milled side-wall has a close to 90° slope, which is crucial to reduce scattering loss from the mechanical boundaries. It is worth to note that the gold residue on the side-wall is caused by the misalignment of electrode. In addition, stress can build up at anchors during the fabrication process. Ion-milled trenches around the signal pad isolate the anchor bases, thereby providing stress relief and electrical isolation. Fig. 2 indicates that the structure has no evidence of buckling or bowing.

Electrode Configuration Trade-offs

The IDT has impact on many aspects of the performance of LN contour-mode resonators. First of all, the mass loading effect from the electrodes can shift the resonator frequency, while the scattering of acoustic wave by acoustic-impedance mismatched electrodes and the electrode material acoustic loss can degrade the quality factor. Second, the metallization ratio and electrode location with respect to the mechanical mode affects the overlap integral between the excitation field profile and the mechanical mode profile, therefore affect the k_t^2. Finally, the relative phase of scattering from electrodes and device boundaries can lead to resonance at undesired parasitic modes. Here, we discuss the resonator performance from two different kinds of electrode placement, namely the type with electrodes placed at mechanical anti-nodes (AN type) and the type with electrodes placed at the mechanical nodes (N type).

Traditionally, the IDT for AlN CMRs are placed at nodal points with a bottom ground plane to couple the vertical electric field to lateral strain though the d_{31} piezoelectric strain coefficient, as the z-axis of sputtered AlN thin film tends to align along the wafer normal direction. On the other hand, AlN FBARs and electrostatic drive MEMS resonators use excitation located at anti-nodes. In contrast, optimum k_t^2 for Y136 LN is realized by exciting the S_0 Lamb mode using IDT placed on the top surface, while the location of the electrodes plays an essential role on the performance of the resonator. Fig. 4 shows the cross-section of resonators with the AN type and N type electrode. The total width of the resonator is $N\lambda/2$. Both electrode configurations have a metallization ratio of 1, λ/4 finger pairs and a period of λ/2, however the AN type has two λ/8 fingers right at the edges of the device. For a SAW device, the IDT has a frequency response of sinc function [7]. However, the sharply defined mechanical boundaries of the CMR form an equivalent mechanical Fabry-Perot (FP) cavity. Therefore, the IDT for CMR has a frequency response of sinc function combined with the frequency response of the FP cavity. For the AN type, the boundary conditions from the device geometry coincides with that from the electrode finger centers. Therefore, the two sets of boundary conditions both reinforce the mechanical mode defined by the wavelength of λ. In contrast, the boundary conditions are misaligned for the N type. Thus, the mode corresponds to λ is extinguished, while the next lower order mode and the next higher order mode are excited (A detailed analysis will be presented in a follow-up journal paper).

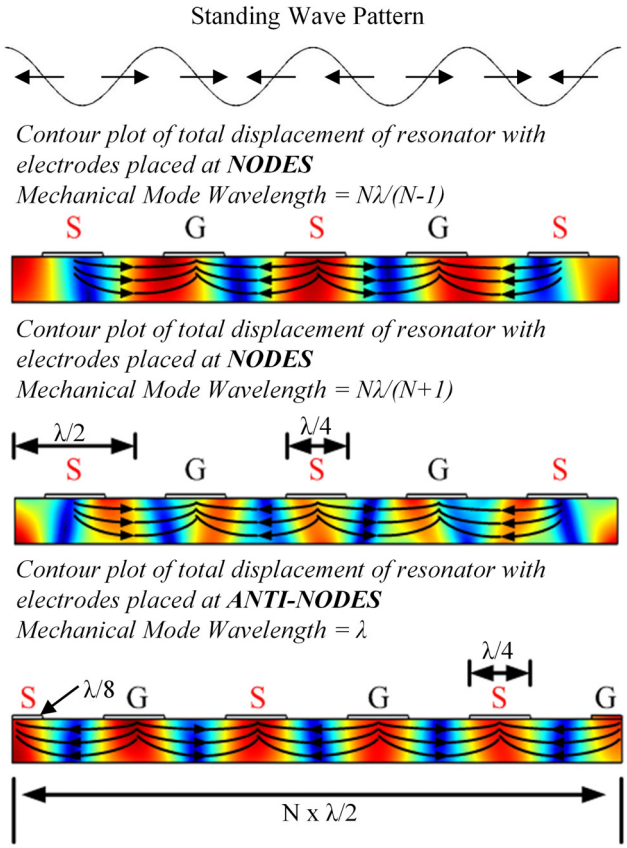

Figure 4: Cross-section of resonators on Y136 LN with electrodes placed at anti-nodes and electrodes placed at nodes, the crystal x-axis is pointing out of the paper. The contour plots show the total displacement of different order modes, the top figure is the standing wave pattern of the Nλ/(N-1) mode with arrows pointing the direction of motion.

Moreover, the excitation E-field profile from the AN type electrodes has a better overlap with the excited mechanical mode (Fig. 4), while the overlap is reduced for N type because of the shift of electrode with respect to the device boundaries (This can be directly noted by comparing the standing wave pattern and the electric field pattern for the *Nλ/(N-1)* in Fig. 4). Therefore, the AN type will also exhibit better k_t^2 comparing to the N type. The drawback of the AN type is that the material loss from the electrode loads the resonator, because of the large compression and stretching motion at the anti-nodes, while the nodal configuration has higher *Q* by offsetting the IDT from points of maximum displacement.

Displacement and Vacuum Testing

Because of the high coupling coefficients and relatively small elasticity coefficients, a small RF power can cause large displacement from LN CMR. For example, a -6dBm RF drive power is sufficient to cause >1nm lateral displacement, while the AlN counterparts moves 50 times less. The displacement from LN CMR is within one order of magnitude of air mean-free-path in room pressure (70nm), putting the device quality factor in the Couette damping limited regime in air. Therefore, comparing to

other technologies, going from air to vacuum can significantly improve the Q of LN CMR.

DEVICE CHARACTERIZATION

Quality Factor vs. Pressure

The performance of the 1-port resonators are measured using N5230A network analyzer. The quality factors are calculated using the Ruby/Avago method [8], and the k_t^2 is measured using the definition as

$$k_t^2 = 1 - f_s^2 / f_p^2 \quad (1)$$

Fig. 5 shows the measured admittance (magnitude and phase) of a 462MHz 'nodal IDT' resonator in air and vacuum (5.4×10^{-3} mbar). The phase transition of the device shows a clear switch from +90° to -90°.The impedance (R_s) at the series peak is 51 Ohm in air and 36.5 Ohm in vacuum, with a k_t^2 of 7%. The quality factor of the series peak is 1500 in air, comparing to 2150 in vacuum. The improvement in Q arises from reduction of Couette damping in vacuum. To further verify the device is Couette damping limited, we also measured Q versus pressure which exhibits clear signature of Couette damping (Fig. 6). This Q improvement from air to vacuum, along with the 7% k_t^2 results in a $k_t^2 \times Q$ of 148 for CMR resonators.

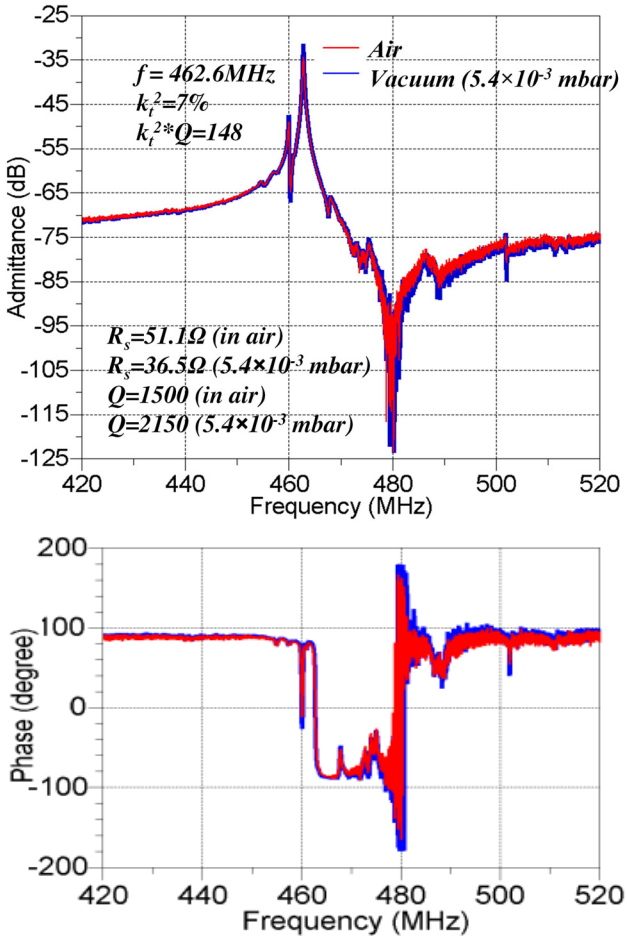

Figure 5: Measured admittance of a 462 MHz "Nodal IDT" resonator measured in vacuum and air. MilliTorr vacuum improves the Q by 30%, resulting in the FOM of 148, which surpasses that of AlN CMRs.

Anti-nodal Electrodes vs. Nodal Electrodes

Fig. 7 shows the measured admittance (in vacuum) of an AN type resonator and a N type resonator. The total widths of both devices are 11/2λ, where λ is 7.6um. As discussed before, the AN type device only shows one main peak at 787.9 MHz, which corresponds to the 7.6 um wavelength. The device shows an excellent k_t^2 of 12.3% and significantly fewer spurs. However, the Q is 650, lower than the N type because of the loading from material loss of Au. In comparison, the nodal configuration shows two strong resonance peaks corresponds to the $N\ \lambda/(N-1)$ mode and the $N\ \lambda/(N+1)$ mode. The frequencies of the two modes are 741.5 MHz and 912.8 MHz. Both modes show higher Q of ~1,000. The k_t^2 of the 741 MHz mode is 8.3%, and the k_t^2 of the 912.8 MHz is 3.1%, which is caused by the smaller overlap between the excitation field and mechanical mode profile. Ideally, the $N\ \lambda/(N-1)$ mode should have a frequency of $(N-1)f_0/N$, where N is the total periods of the device and f_0 is the frequency of the main resonant peak of the AN type. However, the measured frequencies of the N type are higher than that predicted by the theory. This is because the frequency shift caused by the mass loading from the electrode is less for the N type devices. It's also worth to note that the acoustic scattering from the electrodes also contributes to spurious N type spectrum.

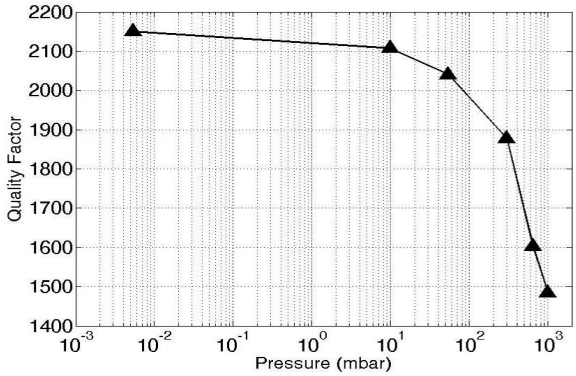

Figure 6: Q of the 462 MHz resonator vs. Pressure showing clear signature of Couette damping.

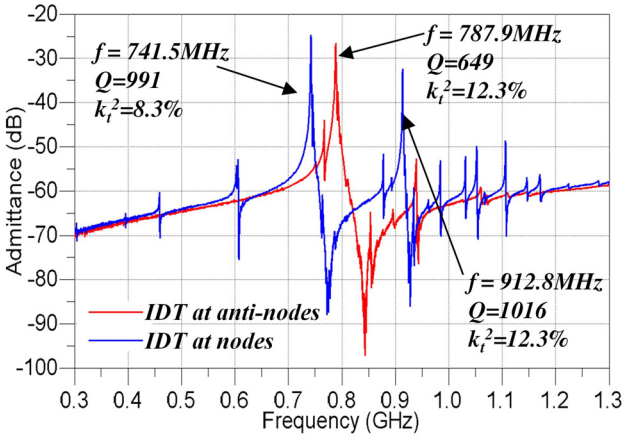

Figure 7: Measured admittance of the two configurations in vacuum. While the nodal configuration has higher series Q, the anti-node configuration has significantly fewer spurs and exceptional coupling coefficient.

Comparison to State of Art

By employing different electrode configurations and using different device dimension, we were able to demonstrate CMRs with different frequencies, quality factors and k_t^2. Fig. 8 shows a microphotograph of one corner (2.4mm x 1.9mm) of a single chip. At the upper right corner, the two devices have a wavelength of 11.2um. The resonant frequency for the AN type is 514.2MHz with a Q of 1100 and k_t^2 of 11.5%, while the N type shows lower resonant frequency and k_t^2, but higher Q. Similarly, the lower left corner shows two devices with wavelength of 7.6 um.

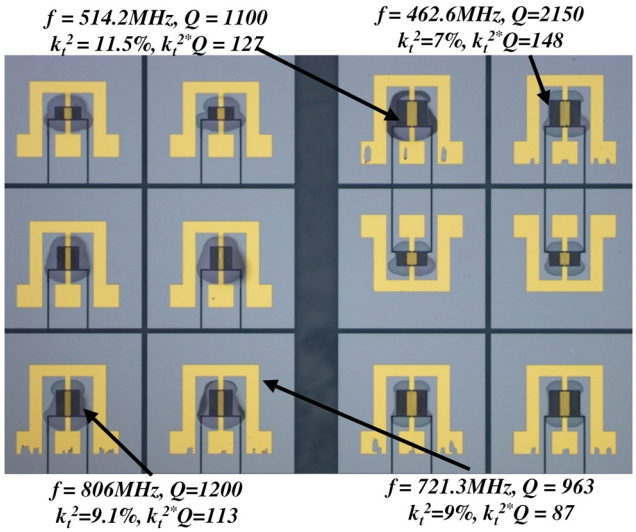

Figure 8: Microphotograph of one corner (2.4mm x 1.9mm) of a single chip, on which device resonances are defined at different frequencies by photolithography (Measured performance for sample resonators are annotated).

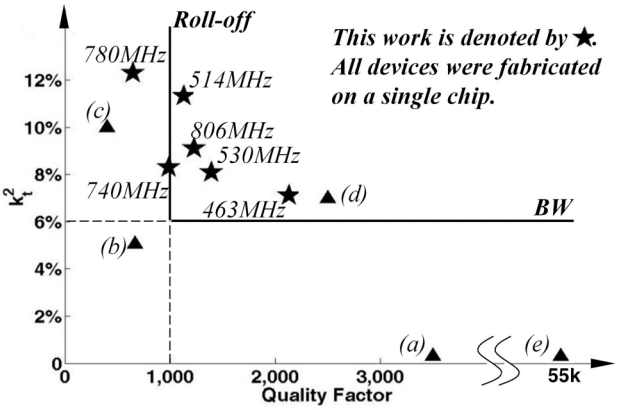

Figure 9: Electromechanical coupling factor vs. quality factor. For RF filters, the k_t^2 determines the maximum possible BW, while the Q determines the filter roll-off. (a) F. Ayazi, sidewall AlN resonator; (b)G. Piazza, ion-sliced LN thin-film resonator [6]*; (c)K. Hashimoto, $LiTaO_3$ SAW; (d) R. Ruby, AlN FBAR* [2]*; (e)Nguyen et al, diamond disk* [1]*; (★) This work.*

Fig. 9 summarizes devices on a single chip with different performances. The resonant frequencies range from 514 MHz to 806 MHz, while the highest k_t^2 achieved on this chip is 12.3%. The quality factor ranges from 700 to 2150. Comparing to other technologies, our device shows sufficient quality factor to achieve fast roll-off comparable to traditional MEMS resonators, meanwhile provides much higher k_t^2 for wide BW operation. In addition, the great versatility of our devices can facilitate single chip integration of devices with different frequencies.

CONCLUSION

With the flexibility of IDT configuration and lithography-defined resonator geometry, we demonstrated, on a single chip, resonators with a wide range of performance (Fig. 8). The $k_t^2 \times Q$ goes up to 148, k_t^2 to 12.3% and Q to 2150. For RF filters, the k_t^2 determines the maximum possible BW, while the Q determines the steepness of the filter roll-off. Comparing to other technologies (Fig. 9), we can achieve both high Q and high k_t^2, and more importantly provide the flexibility to integrate multi-frequency resonators and filters on a single chip.

ACKNOWLEDGEMENTS

The authors wish to thank The authors wish to thank the DARPA ART program, whose generous grant has made this research possible. We would also like to thank Dr. Seungbae Lee, Professor Sheng-Shian Li, Dr. Warren Welch, and Dr. Jason Reed for initial work on LN resonator and process development.

REFERENCES

[1] J. Wang, J. E. Butler, T. Feygelson, and C. T. Nguyen, "1.51-GHz nanocrystalline diamond micromechanical disk resonator with material-mismatched isolating support", *IEEE MEMS 2004*, pp. 641-644.

[2] R. Ruby, P. Bradley, J. Larson, Y. Oshmyansky, and d. Figueredo, "Ultra-miniature high-Q filters and duplexers using FBAR technology," *ISSCC 2001,* pp. 120-121.

[3] G. Piazza, P. J. Stephanou, J. P. Black, R. M. White, and A. P. Pisano, "Single-chip multiple-frequency RF microresonators based on Alumium Nitride contour-mode and FBAR technologies", *Ultrasonics 2005*, 1187 (2005).

[4] M. Kadota, T. Kimura, and Y. Ida, "Ultra wide band resonator composed of grooved Cu-electrode on $LiNbO_3$ and its application to tunable filter", *Ultrasonics 2009*, pp. 2668-2671.

[5] R. Wang, S. A. Bhave, and K. Bhattacharjee, "Thin-film Lithium Niobate contour-mode resonators", *Ultrasonics 2012*.

[6] S. Gong, L. Shi, and G. Piazza, "High electromechanical coupling MEMS resonators at 530 MHz using ion sliced X-cut $LiNbO_3$", *IMS 2012*.

[7] M. Kadota, et al., "Very small IF resonator filters using reflection of shear horizontal wave at free edges of substrate", *Tran. UFFC*, pp. 1269-1279, 49 (2002).

[8] R. Ruby, et al., "After 60 years: A new formula for computing quality factor is warranted," *Ultrasonics 2008,* pp. 431-436.

CONTACT

*Renyuan Wang, tel: +(001)607-793-0877; rw364@cornell.edu